

JCTC

Journal of Chemical Theory and Computation

Automated Parametrization of Biomolecular Force Fields from Quantum Mechanics/Molecular Mechanics (QM/MM) Simulations through Force Matching

Patrick Maurer, Alessandro Laio,[†] Håkan W. Hugosson,[‡] Maria Carola Colombo, and Ursula Rothlisberger*

École Polytechnique Fédérale de Lausanne (EPFL), Institute of Chemical Sciences and Engineering, BCH-LCBC, CH-1015 Lausanne, Switzerland

Received September 14, 2006

Abstract: We introduce a novel procedure to parametrize biomolecular force fields. We perform finite-temperature quantum mechanics/molecular mechanics (QM/MM) molecular dynamics simulations, with the fragment or moiety that has to be parametrized being included in the QM region. By applying a force-matching algorithm, we derive a force field designed in order to reproduce the steric, electrostatic, and dynamic properties of the QM subsystem. The force field determined in this manner has an accuracy that is comparable to the one of the reference QM/MM calculation, but at a greatly reduced computational cost. This allows calculating quantities that would be prohibitive within a QM/MM approach, such as thermodynamic averages involving slow motions of a protein. The method is tested on three different systems in aqueous solution: dihydrogenphosphate, glycyl–alanine dipeptide, and a nitrosyl–dicarbonyl complex of technetium(I). Molecular dynamics simulations with the optimized force field show overall excellent performance in reproducing properties such as structures and dipole moments of the solutes as well as their solvation pattern.

1. Introduction

Molecular dynamics (MD) simulations using empirical force fields have become a standard tool to investigate the structure and dynamics of biological systems, such as proteins, nucleic acids, and membranes.¹ A variety of force fields tailored for biomolecular applications have been developed over recent decades, and they are still being continuously improved^{2–5} (for a recent detailed overview, see refs 6 and 7).

These force fields provide parameters for simulating standard proteins, nucleic acids, lipids, some cofactors, and a number of solvents, so that a large variety of biological systems can routinely be studied. Often, however, one would

like to simulate systems containing molecules or moieties for which force field parameters are not available. Examples include drug/receptor complexes or enzymes and nucleotide sequences that bind to a metal or contain special chemical modifications. The development of a reliable force field for these systems can be a cumbersome and time-consuming task. A common approach consists in deriving parameters from an electronic-structure calculation of the molecule or of a model compound in the gas phase. Atomic point charges are obtained by fitting to the quantum electrostatic potential (ESP) estimated on a grid surrounding the molecule.⁸ The calculation of vibrational properties provides force constants for bonded interactions. Since these calculations are usually performed in the gas phase, polarization effects in the condensed phase are accounted for in a somewhat arbitrary—but nevertheless successful—fashion by using a basis set (6-31G*) that is known to overestimate polarization.⁸ The resulting parameters need to be tested against experimental data and, if necessary, readjusted.

* Corresponding author phone: ++41 (0)21 693 0325; fax: ++41 (0)21 693 0320; e-mail: ursula.roethlisberger@epfl.ch.

[†] Current address: International School for Advanced Studies (SISSA), I-34014 Trieste, Italy.

[‡] Current address: Laboratory of Theoretical Chemistry, Royal Institute of Technology, S-10691 Stockholm, Sweden.

Alternatively, parametrization can be completely circumvented by performing hybrid quantum mechanical/molecular mechanical (QM/MM) simulations.^{9–13} In QM/MM simulations, the system is partitioned into a core region (the QM region), which is treated with a quantum chemical method, usually density functional theory (DFT) or semiempirical approaches, and an environment (the MM region) described with a classical force field. The QM region can be chosen in such a way that it includes all components of the system for which no parametrization is available. The QM/MM approach allows for an accurate description of the QM region under the steric and electrostatic influence of the environment. However, the high degree of accuracy is achieved at the price of a significant computational cost.

Ideally, one would like to perform simulations with the accuracy of a QM/MM treatment at the computational cost of classical MD. With this goal in mind, we propose here to exploit QM/MM simulations for deriving a force field designed in such a way as to reproduce the steric, electrostatic, and dynamic properties of the QM subsystem. In the QM/MM implementation used in this work,¹³ the charge density of the quantum region is explicitly polarized by the electric field generated by the atomic point charges of the classical environment. In addition, effects such as temperature and pressure are automatically taken into account.

The force field determined in this manner can be used to efficiently sample the configurational space without the severe limitations of the simulation time of first-principles-based QM/MM schemes. This allows the calculation of, at a low computational cost, quantities that would be prohibitive within a QM/MM approach, such as, for the ligand docking problem, thermodynamic averages involving slow motions of the target protein. The potential constructed by this method is tailored for the long-time propagation of a specific system. As a consequence, the transferability of this tailored force field is expected to be limited. For example, the parameters determined with this method for the same solute solvated in water or acetone might be different and not necessarily transferable between the two cases. This approach resembles the optimal potential method¹⁴ and the “learn-on-the-fly” approach,¹⁵ introduced a few years ago for solid-state physics applications. A more transferable potential can be obtained by choosing several reference systems, with, for example, different solvents or different protein environments.

As one of the reviewers of this article pointed out, using conformations from QM/MM simulations to generate ESP-derived charges has an additional advantage over the traditional use of gas-phase optimized structures. Especially in the case of highly polar species, gas-phase optimized structures are usually “closed-up”, for example, as a result of the formation of intramolecular hydrogen bonds, which leads to nontransferable charges. The explicit hydration of such species allows for breaking intramolecular hydrogen bonds, resulting in more “open” conformations and more transferable charges.

In the work presented here, the parameters are derived exploiting the so-called force-matching technique. This approach dates back to the work of Ercolessi and Adams,¹⁶ who developed an empirical potential for aluminum by fitting

the parameters so as to reproduce a set of forces obtained from *ab initio* calculations. Force matching has since been applied with great success to parametrize empirical potentials for several systems of increasing complexity. Examples include Fe,¹⁴ Si/SiO₂,^{15,17,18} tantalum,¹⁹ alkaline earth oxides,^{20,21} and H₂O.²²

Here, we apply force matching to parametrize a standard, nonpolarizable, biomolecular force field, without any modifications of the functional form. We optimize all of the charges and torsional, bonding, and bending parameters. The Lennard-Jones parameters are not optimized but are kept fixed to the standard force field value. This choice is consistent with the QM/MM interaction Hamiltonian we use that retains the Lennard-Jones parameters from the classical force field.¹³ Leaving the functional form unchanged allows for a seamless integration of the fitted parameters for a subregion of the system into an accurate and well-tested existing set of parameters for the surrounding protein. The choice of a nonpolarizable force field has been motivated by the following reasons. Although there is consensus in the field that the explicit inclusion of polarization plays an important role in the development of more accurate force fields,^{6,7} and considerable success has already been achieved,^{23–32} such force fields cannot yet be considered standard methods. Using a nonpolarizable force field provides an accuracy benchmark against which more sophisticated models can be compared. The force-matching procedure can thus be used to identify situations where a higher-level force field leads to an important improvement, as opposed to situations where a minor improvement would not justify the additional computational cost.

In this work, the fit is performed using finite-temperature QM/MM trajectories of a few picoseconds. During this relatively short simulation time, it is unlikely to observe a dihedral transition in the QM subsystem. Therefore, the procedure described in this work provides a parameter set that can be safely used only for a specific conformer of the system. It is possible to generate a force field that also reproduces torsional barriers if the QM/MM dynamics are performed under the action of a bias potential that induces transitions in the available computational time.^{33–36}

We will show that, after reparametrization, a standard, nonpolarizable, biomolecular force field performs in fact remarkably well in reproducing QM/MM results even for an electronically complex compound such as a nitrosyl–dicarbonyl complex of technetium(I).

2. Methods

The parametrization of a force field for a subregion of a system is carried out in three steps: First, a QM/MM simulation at finite temperature is performed, with the fragment to be parametrized being included in the QM subsystem. During this simulation, the forces on all the atoms of the QM subsystem as well as the electrostatic potential and field on the nearby MM atoms are stored. Second, a set of atomic point charges $\{q_i\}$ that reproduce the electrostatic potential and forces that the QM system exerts on the surrounding classical atoms is derived. Third, the nonbonded contributions, computed with the charges obtained in the

second step and given Lennard-Jones parameters, are subtracted from the total forces on the QM atoms. The remaining forces are assumed to be derived from bonded interactions. The parameters for bonded interactions (torsions, bending, and bonds) are thus adjusted in order to reproduce the remaining forces. The entire procedure is described in detail in the following sections.

2.1. Reference Forces. The force field for a fragment is optimized, requiring that the classical forces reproduce a set of forces computed in configurations generated by a finite-temperature QM/MM molecular dynamics run. The MM and QM subsystems are explicitly coupled by a potential that describes their steric and electrostatic interaction.¹³ The QM subsystem is treated at the DFT level, with classical atoms within a distance of 8 Å being explicitly coupled to the quantum charge density. Additional coupling schemes for more distant MM atoms, for example, via classical point charges or multipole expansion of the density,¹³ were not used in order to facilitate the derivation of atomic point charges (see below in section 2.2.1).

The method is tested by generating force fields for three different molecules in aqueous solution. The three test systems and the corresponding computational setups are detailed in section 2.3. In all three cases, the QM subsystem consists of the solute molecule to be parametrized, while the surrounding solvent is treated at the classical level. Thus, all interactions between the QM and MM subsystems are of a nonbonded nature. For each system, a second QM/MM trajectory is generated for validating the newly generated force field and assessing its accuracy.

2.2. Force Matching. We perform the fitting procedure with the GROMOS96 functional form² for the classical force field. The potential energy E_p is given by the sum of the nonbonded potential E_p^{nb} and the bonded (covalent) potential E_p^{b} , where E_p^{nb} is given by (in atomic units)

$$E_p^{\text{nb}} = \sum_i^N \sum_j^{N_i^{\text{nb}}} \left(\frac{q_i q_j}{r_{ij}} + \frac{A_{ij}}{r_{ij}^{12}} - \frac{B_{ij}}{r_{ij}^6} \right) \quad (1)$$

The index i runs over all N atoms in the system, while the index j runs over all N_i^{nb} atoms within a cutoff distance r_c of atom i , excluding first and second neighbors, that is, atoms that are connected to i by one or two covalent bonds. q_i and q_j are fractional atomic point charges. A_{ij} and B_{ij} are the coefficients of the Lennard-Jones potential between atoms i and j . The contribution E_p^{b} is given by

$$E_p^{\text{b}} = \sum_{n=1}^{N^{\text{bon}}} \frac{1}{4} k_b (b_n^2 - b_{0n}^2)^2 + \sum_{n=1}^{N^{\text{ang}}} \frac{1}{2} k_{\theta n} (\cos \theta_n - \cos \theta_{0n})^2 + \sum_{n=1}^{N^{\text{imp}}} \frac{1}{2} k_{\xi n} (\xi_n - \xi_{0n})^2 + \sum_{n=1}^{N^{\text{tor}}} k_{\varphi n} [1 + \cos(\delta_n) \cos(m_n \varphi_n)] \quad (2)$$

The first term assigns a bond-stretching potential with force constant k_b to all atom pairs connected by a covalent bond and keeps the bond length b close to its equilibrium value b_0 . The second term keeps bond angles θ close to an equilibrium value θ_0 . The third term corresponds to a harmonic (or so-called improper) dihedral angle potential and

is used to maintain the planarity of groups such as sp^2 -hybridized carbon atoms. The fourth term represents a periodic torsional potential with a barrier height of $2k_\varphi$ and a phase-shift δ (0 or π). m is the multiplicity, that is, the number of minima in the interval $[-\pi, \pi]$.

The force matching is performed in two separate steps: first, the nonbonded parameters (i.e., atomic charges) are optimized, and in a subsequent step, the parameters for bonded interactions are optimized.

2.2.1. Fit of Atomic Point Charges. The method to derive atomic point charges is closely related to the method of dynamically generated electrostatic-potential-derived charges (D-RESP) introduced by Laio et al.³⁷ In the D-RESP method, the grid used for charge fitting is defined by the positions of all classical atoms that are explicitly coupled to the QM charge density (the so-called NN atoms).^{13,37} Since QM/MM coupling requires the computation of the electrostatic potential on the NN atoms at each step of a QM/MM simulation,¹³ the charges can be derived “on-the-fly” with minimal computational overhead, in a single computational step that consists in solving a system of linear equations.³⁷ This step also introduces a restraint of the atomic charges to their Hirshfeld values.³⁸ Such a restraint is necessary as unrestrained fitting results in an overdetermined problem for which many nearly equivalent solutions exist, leading to charge sets that are purely “best-quality-of-fit”, with values that are often chemically not meaningful and show a strong dependence on the conformation of the molecule.^{8,37}

Here, we have modified the original D-RESP scheme in a few important aspects. In order to reproduce in the best possible manner the solvation structure around the QM subsystem, we require the charge set to also reproduce the electric field on the NN atoms originating from the QM charge density, in addition to the potential. Chemically equivalent atoms, such as the hydrogen atoms of a methyl group, are required to carry identical charges. While D-RESP charges are derived at each MD step, we here derive from the QM/MM trajectory a single set of charges that performs best on average over all reference conformations used for the fit. It was shown by Reynolds et al. that including multiple conformations results in more transferable charges compared to those derived from a single conformation.³⁹ As a welcome side effect, this allows for a weaker restraint to the Hirshfeld charges than is necessary when deriving charges for a single conformation. The set of atomic point charges $\{q_i\}$ is obtained by minimizing a target penalty χ^2 :

$$\chi^2 = \sum_{l=1}^L \left[\sum_{j \in \text{NN}_l} w^V (V_{jl}^{\text{MM}} - V_{jl}^{\text{p}})^2 + \sum_{j \in \text{NN}_l} w^E \|\mathbf{E}_{jl}^{\text{MM}} - \mathbf{E}_{jl}^{\text{p}}\|^2 \right] + \sum_{i \in \text{QM}} w^H (q_i - q_i^{\text{H}})^2 + w^Q (Q^{\text{tot}} - \sum_{i \in \text{QM}} q_i)^2 \quad (3)$$

The index l runs over all L conformations; j runs over all NN_l classical atoms that are explicitly coupled to the quantum system in configuration l , and i refers to atoms of the quantum system. w^V , w^E , w^H , and w^Q are arbitrarily chosen weighting factors whose values will be specified in section 3.1.1. V_{jl}^{p} and $\mathbf{E}_{jl}^{\text{p}}$ are the electrostatic potential and field, respectively, on the classical atom j in configuration l due

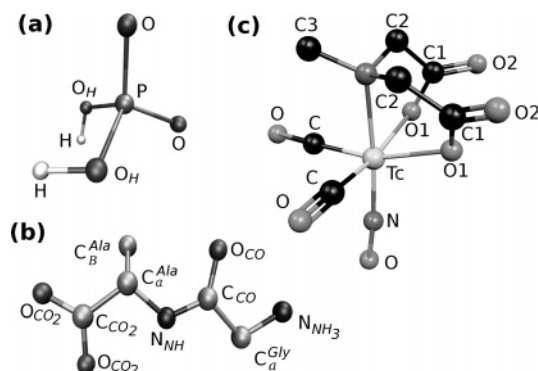


Figure 1. Graphical representation of test compounds and the naming convention used for atom types: (a) H_2PO_4^- , (b) Gly-Ala dipeptide, and (c) TNDM. In b and c, hydrogen atoms have been omitted for clarity.

to the presence of the QM system, while V_{jl}^{MM} and $\mathbf{E}_{jl}^{\text{MM}}$ are the potential and field resulting from the classical point charges $\{q_i\}$. The third term in eq 3 restrains the charges q_i to the Hirshfeld charges q_{il}^{H} , and the last term finally restrains the total charge of the subsystem to the correct value Q^{tot} . The minimization of χ^2 corresponds to solving an overdetermined⁴⁰ system of linear equations in $\{q_i\}$ in the least-squares sense, a task that can conveniently be solved with an algorithm such as *QR* factorization.⁴¹ The original D-RESP scheme is recovered by choosing values $L = 1$, $w^{\text{V}} = 1$, $w^{\text{E}} = 0$, and $w^{\text{H}} = 0.1$.³⁷

2.2.2. Bonded Interactions. In a second step, the set of charges $\{q_i\}$ is used to calculate the total nonbonded forces on all of the QM atoms, taking into account exclusions and a scaling of 1–4 interactions² according to the GROMOS96 functional form. We denote these forces by $\mathbf{F}_i^{\text{MMnb}}$ (for the QM atom i and the configuration l). The set of parameters $\{x_n\} = \{b_{0n}, \theta_{0n}, k_{bn}, k_{\theta n}, k_{\xi n}, k_{\varphi n}\}$, describing bonded interactions, is then determined by minimizing the function σ^2 , given by

$$\sigma^2 = \sum_{l=1}^L \sum_{i \in \text{QM}} \|\mathbf{F}_i^{\text{MMnb}} - (\mathbf{F}_i^{\text{QM}} - \mathbf{F}_i^{\text{MMnb}})\|^2 \quad (4)$$

The minimization of σ^2 corresponds to a nonlinear least-squares optimization. Since the derivatives $\partial\sigma/\partial x_n$ are trivial to calculate analytically, a gradients-based optimization algorithm can be used. Specifically, we use the Levenberg–Marquardt algorithm as implemented in the MINPACK collection of routines.^{42,43}

2.3. Test Systems. The method is validated through simulations of aqueous solutions of three different molecules. Their structures and the naming scheme used for atom types are shown in Figure 1. In all three test cases, the QM subsystem consists of the molecule to be parametrized, while the surrounding solvent is treated at the classical level. The three test cases are as follows:

(i) *The Anion Dihydrogenphosphate (H_2PO_4^-).* H_2PO_4^- is used as a prototype for the functional group $\text{R}-\text{PO}_4-\text{R}'$ that is ubiquitous in biomolecules. Since it is an anion, the solvent is expected to significantly polarize the system.

(ii) *The Zwitterionic Form of the Dipeptide Glycyl-Alanine (Gly-Ala).* In previous work,⁴⁴ we have compared the

solvation structure of this dipeptide at different levels of theory, from classical MD to QM/MM to a full QM treatment of the dipeptide and its first and second solvation shells. It was found that classical simulations with the Amber/parm94 and GROMOS96 force fields exhibit significant differences in the solvation structure, compared to QM/MM and full QM simulations, especially for the charged termini. This system thus provides a suitable test to show that reparametrization can improve the solvation properties with respect to a (higher-level) reference simulation.

(iii) *The Transition Metal Complex $[\text{Tc}(\text{NO})(\text{CO})_2(\text{MIDA})]$ (MIDA = *N*-Methyl-iminodiacetic Acid) (TNDM).* Technetium compounds are used in nuclear medicine for the diagnosis and localization of tumor cells, while their rhenium analogues have potential use in therapeutic intervention.⁴⁵ The $[\text{Tc}(\text{NO})(\text{CO})_2]^{2+}$ core is thought to be highly promising for the labeling of biomolecules, because of its small size and low molecular weight.⁴⁶ The generation of force field parameters for this compound enables the investigation of interactions between labeled biomolecules and their biological targets by means of well-established techniques within the framework of classical MD simulations. We consider this compound an excellent test case for our approach, as it presents a number of challenging features, such as metal–ligand bonds and subtle differences between the isoelectronic ligands CO and NO^+ . Moreover, the complex is highly inert, so that a description of metal–ligand bonds by simple harmonic potentials appears justified.

2.3.1. Computational Details. The QM/MM implementation used in this work¹³ combines the packages CPMD^{47,48} for the quantum system and GROMOS96⁴⁹ for the classical part. The QM subsystem is treated at the DFT level, using norm-conserving pseudopotentials of the Martins–Trouiller type.⁵⁰ The plane-wave basis was expanded up to a cutoff of 70 Ry. Classical atoms within a distance of 8 Å were explicitly coupled to the quantum charge density.¹³ All simulations were performed at 300 K under constant volume conditions.

System sizes and simulation times were as follows. (i) H_2PO_4^- : cubic quantum box with an edge of 9 Å; BLYP exchange-correlation functional^{51,52} for the QM subsystem; MM subsystem consisting of 763 water molecules (SPC model⁵³) in a cubic box with an edge of 14 Å; a total QM/MM simulation time of 20 ps, of which 7 ps were used for parametrization and 13 for validation. (ii) Gly-Ala dipeptide: quantum box of size 15 × 12 × 12 Å³; BLYP functional; MM subsystem consisting of 1718 water molecules (SPC) in a cubic box with length 37 Å; 3 ps of QM/MM simulation used for parametrization and 7 for validation. (iii) TNDM: cubic quantum box with length 14 Å; BP86 exchange-correlation functional,^{51,54} which for Tc compounds provide a better agreement with experimental structures;⁵⁵ MM subsystem consisting of 1663 water molecules (TIP3P model⁵⁶) in a cubic box with length 37 Å; 3 ps of QM/MM simulation for parametrization and 4 for validation. The standard GROMOS force field does not provide Lennard–Jones parameters for Tc^+ and the nitrosyl ligand. Since our goal was to validate the force-matching procedure, and Lennard–Jones interactions are treated identically in the QM/

MM and classical calculations, we decided to avoid large computational efforts for an accurate determination of these parameters. Instead, an ad hoc approach was chosen to determine the missing parameters: The nitrogen and oxygen atoms of the nitrosyl ligand were assigned the parameters of an amine nitrogen and a carbonyl oxygen, respectively. For technetium, we used the parameters describing a Cu^+ ion, because the charges are identical and, among those metal ions for which the standard force field provides parameters,² Cu^+ is most similar in size to Tc^+ . For simulations of TNDM for purposes other than validation of the force-matching approach, the missing Lennard-Jones parameters clearly need to be determined in a more careful fashion.

In order to probe the influence of explicit solvation on the charges, an additional set of charges was derived from the electrostatic potential calculated in the gas phase. These charges were derived according to the RESP scheme,⁸ but using solute structures from the QM/MM simulations instead of gas-phase optimized ones. Gaussian 03⁵⁷ was used to perform single-point HF/6-31+G* calculations, and the program resp from the Amber suite⁵⁸ was used to compute the RESP charges.

For each set of fitted parameters, a classical MD run was performed to generate a trajectory to be compared to the QM/MM reference. Initial coordinates and velocities, the time step, and total simulation time were all chosen to be identical to those of the corresponding QM/MM trajectory used for validation.

3. Results and Discussion

3.1. Quality of Fit. **3.1.1. Electrostatics.** To measure the quality of a charge set $\{q_i\}$, we compute the relative standard deviation (SD) of the electrostatic potential (SD_V) and field (SD_E) with respect to the QM reference values over all L configurations, with SD_V and SD_E defined as

$$\text{SD}_V = \sqrt{\frac{\sum_l \sum_{j \in \text{NN}_l} (V_{jl}^{\text{MM}} - V_{jl}^{\text{Q}})^2}{\sum_l \sum_{j \in \text{NN}_l} (V_{jl}^{\text{Q}})^2}} \quad (5)$$

$$\text{SD}_E = \sqrt{\frac{\sum_l \sum_{j \in \text{NN}_l} \|\mathbf{E}_{jl}^{\text{MM}} - \mathbf{E}_{jl}^{\text{Q}}\|^2}{\sum_l \sum_{j \in \text{NN}_l} \|\mathbf{E}_{jl}^{\text{Q}}\|^2}} \quad (6)$$

In order to probe the influence of the weighting parameters in eq 3, a series of charge sets were derived for different values of w^V , w^E , w^H , and w^Q . The results for H_2PO_4^- are shown as a representative example in Figure 2a.

As expected, increasing the weight w^E improves the quality of the electric field, that is, of the forces on the MM atoms. However, this is achieved at the price of a poorer quality of the electrostatic potential. Moreover, high values of w^E in combination with a weak restraint to Hirshfeld charges (i.e.,

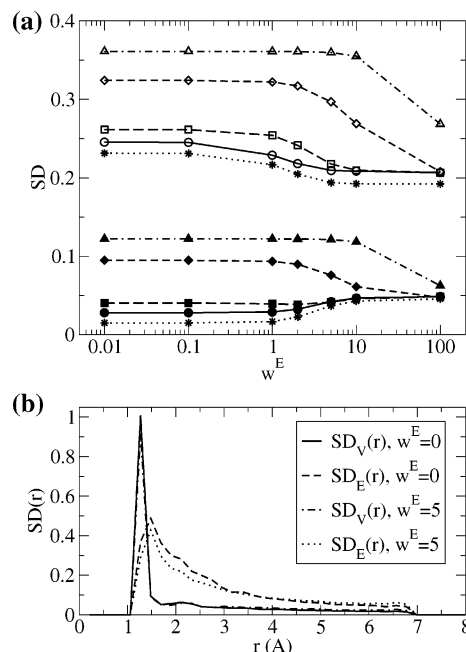


Figure 2. (a) SD_V (filled symbols) and SD_E (empty symbols) for H_2PO_4^- as a function of w^E for different values of w^H : 0 (circles), 0.01 (squares), 0.1 (diamonds), and 1.0 (triangles). $w^V = 1$ and $w^Q = 1000$ in all cases. Stars indicate the best possible quality of fit mentioned in the text. (b) SD_V and SD_E as a function of distance to the nearest QM atom. $w^H = 0.01$.

small w^H) lead to considerable deviations of the total charge from its correct value, an effect that was found to be especially strong in the case of H_2PO_4^- . This behavior is remedied by restraining the overall charge to the correct value through a high value of w^Q . The effect does not occur when fitting the potential only, so that the above constraint is not needed when $w^E = 0$ (as in the original D-RESP procedure).

Remarkably, the fit can only be marginally improved by allowing for fluctuating charges. Star symbols in Figure 2a indicate the average SD_V and SD_E of charges that were derived for single snapshots, without imposing any equivalencies between atoms. Thus, these charges represent the best quality of fit that can be achieved, for given values of w^V , w^E , w^H , and w^Q , with a polarizable model that uses exclusively atom-centered point charges, such as the fluctuating charge model.^{23,59} This result suggests that the accuracy limiting factor is not so much the use of fixed charges instead of fluctuating ones but that it is rather the model of exclusively atom-centered point charges itself. This view is in agreement with work by Masia et al.,⁶⁰ who showed that polarizable models with additional interaction sites are superior to the fluctuating-charge model in their ability to reproduce the polarization of a quantum system by classical point charges.

Figure 2b shows SD as a function of the distance to the nearest QM atom. As can be seen, the deviation is largest at short distances, and this effect is more pronounced for the field than for the potential. Most likely, these deviations result from the inability of a simple atomic point charge model to describe the highly inhomogeneous field in the immediate vicinity of the QM system. The deviations are very large only for small distances (< 1.7 Å) that correspond to the short-range tail of the radial distribution function of hydrogen

Table 1. Atomic Charges of H_2PO_4^-

atom ^a	MDR	MDRF	D-RESP ^b	RESP ^c
P	+0.011	+0.513	-0.038	+1.547
O	-0.596	-0.658	-0.599	-0.902
O _H	-0.326	-0.580	-0.214	-0.770
H	+0.416	+0.482	+0.336	+0.398

^a Atom types (see Figure 1a). ^b Time-averaged values over the QM/MM reference trajectory. See also ref 62. ^c Gas-phase HF/6-31+G*.

Table 2. Atomic Charges of Gly-Ala

atom ^a	MDR	MDRF	D-RESP ^b	RESP ^c	G96 ^d	Amber ^e
H _{NH₃}	+0.379	+0.444	+0.227	+0.334	+0.248	+0.164
N _{NH₃}	-0.395	-0.658	+0.145	-0.395	+0.129	+0.294
C _{Gly} _α	+0.045	+0.150	+0.039	-0.041	+0.127	-0.010
H _{Gly} _α	+0.081	+0.051	+0.080	+0.132	0.000	+0.090
C _{CO}	+0.544	+0.493	+0.069	+0.591	+0.380	+0.616
O _{CO}	-0.681	-0.593	-0.457	-0.587	-0.380	-0.572
N _{NH}	-0.571	-0.707	+0.083	-0.579	-0.280	-0.382
H _{NH}	+0.417	+0.471	+0.236	+0.313	+0.280	+0.268
C _{Ala} _α	+0.265	+0.472	+0.086	+0.168	0.000	-0.175
H _{Ala} _α	+0.099	+0.013	+0.123	+0.082	0.000	+0.107
C _{Ala} _β	-0.162	-0.164	-0.040	-0.293	0.000	-0.209
H _{Ala} _β	+0.054	+0.035	+0.038	+0.078	0.000	+0.076
C _{CO₂}	+0.710	+0.456	-0.064	+0.861	+0.270	+0.773
O _{CO₂}	-0.865	-0.736	-0.574	-0.810	-0.635	-0.806

^a Atom types (see Figure 1b). ^b Time-averaged values over the QM/MM reference trajectory. See also ref 62. ^c Gas-phase HF/6-31+G*. ^d GROMOS 43A1 force field.² ^e Parm94 force field.³

bonds.⁶¹ Therefore, as we will show in the following, this error in the fit has only a marginal influence on the solvation structure.

Two different sets of parameters were derived via the force-matching procedure: a first one, in which charges were derived by fitting only to the electrostatic potential, that is, $w^E = 0$, and a second one with charges derived from both the potential and the field, with $w^E = 5$. We will refer to the former as MDR (multiconformation D-RESP charges) and to the latter as MDRF (F for field). The remaining weighting factors were in both cases set to $w^V = 1$, $w^H = 0.01$, and $w^Q = 1000$. The charge sets derived from gas-phase HF/6-31+G* calculations (see section 2.3.1) are denoted as RESP. Tables 1–3 compare the MDR and MDRF charges of the three test compounds to RESP and time-averaged D-RESP charges and, in the case of Gly-Ala, also to the values used in the Amber/parm94 and GROMOS96 force fields.

In general, MDR(F) charges are similar to those used in the Amber force field, which is not surprising since both are based on a quantum mechanical origin. The most striking difference is observed for the terminal ammonium group of Gly-Ala, which is strongly polarized in the MDR(F) charge sets. The positive charge of the ammonium group is localized on the hydrogen atoms, while the nitrogen atom carries a negative partial charge. In the Amber and GROMOS force fields, in contrast, the positive charge is more evenly distributed. This difference in charge distribution most likely arises from the fact that MDR(F) charges are derived for an explicitly hydrated species in a condensed system.

The optimized atomic charges for TNDM are shown in Table 3. Compared to the formal charges of Tc^+ , NO^+ , and

Table 3. Atomic Charges of TNDM

atom ^a	MDR	MDRF	D-RESP ^b
Tc	+1.791	+1.664	+1.794
N	-0.353	-0.331	-0.341
O _{NO}	+0.102	+0.090	+0.102
C	-0.231	-0.068	-0.284
O _{CO}	+0.059	-0.056	+0.098
C1	+0.111	+0.479	-0.026
O1	-0.494	-0.661	-0.472
O2	-0.520	-0.580	-0.414
C2	+0.024	-0.069	+0.015
H _{C2}	+0.129	+0.096	+0.131
N1	-0.069	-0.056	-0.051
C3	-0.031	-0.045	-0.017
H _{C3}	+0.048	+0.068	+0.052

^a The naming scheme for atom types is shown in Figure 1c.

^b Average over the QM/MM reference trajectory. See also ref 62.

Table 4. Relative Error of the Total Force SD_T

	MDR	MDRF	G96
H_2PO_4^-	0.44	0.42	1.36 ^a
Gly-Ala	0.28	0.28	1.01 ^b
TNDM	0.34	0.33	N/A

^a See ref 63. ^b GROMOS96 43A1 force field.²

CO, the optimized charges appear to indicate a considerable amount of charge transfer from the metal center to the nitrosyl and carbonyl ligands. This result can be interpreted as a manifestation of the known strong π back donation from metal d orbitals into antibonding π^* orbitals of these ligands, resulting in metal–ligand bonds of highly covalent character.

3.1.2. Bonded and Total Forces. In analogy to SD_E in eq 6, we define standard deviations SD_B to measure the quality of the bonded forces and SD_T to measure the quality of the total force. Bonded forces are reproduced with values of SD_B between 0.24 (Gly-Ala) and 0.28 (TNDM). The relative errors in the total force SD_T are shown in Table 4. Both charge sets yield similar SD_T values for a given molecule, with MDRF parameters outperforming MDR by a few percent. The error is largest in the case of H_2PO_4^- with $\text{SD}_T = 0.44$, and the best performance is obtained in the case of Gly-Ala with $\text{SD}_T = 0.28$. Interestingly, when looking at the SD_T per atom in Gly-Ala, the largest error is made on the oxygen atoms with $\text{SD}_T = 0.4$, similar in size to that in H_2PO_4^- . These findings are a clear indication that the main source of error lies in the description of electrostatics with a simple, atom-centered, point-charge model. This simplification will have the strongest impact when the charge distribution around an atom is anisotropic, as is the case with lone pairs located on oxygen atoms.

3.2. MD with Optimized Parameter Sets. 3.2.1. Solvation Structure. The ability to reproduce the solvation structure of the reference QM/MM simulation provides a sensitive test for the quality of the optimized charge sets. The solvation structure is analyzed by calculating radial distribution functions $g(r)$ between solute and solvent atoms. We denote water oxygen and hydrogen atoms as O_W and H_W , respectively.

Figure 3 compares radial distribution functions $g(r)$ of the phosphate ion in water. The corresponding coordination

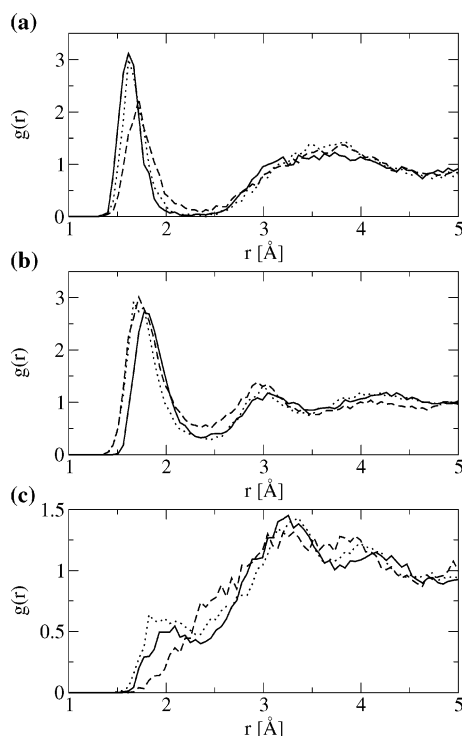


Figure 3. Radial distribution functions $g(r)$ of H_2PO_4^- in water. Solid lines indicate the QM/MM reference simulation; dashed lines indicate the simulation with the charge set MDR, and dotted lines indicate the one with the charge set MDRF. Shown are the radial distribution functions (a) $\text{H}-\text{O}_\text{W}$, (b) $\text{O}-\text{H}_\text{W}$, and (c) $\text{O}_\text{H}-\text{H}_\text{W}$. The names of the atom types are shown in Figure 1a.

Table 5. Hydrogen-Bond Coordination Numbers N_C (per Atom) for the First Solvation Shell of H_2PO_4^- (Top) and Gly-Ala (Bottom)

	QM/MM	MDR	MDRF	RESP	G96
H	1.0	1.0	1.0	1.0	N/A
O_H	1.4	1.5	1.7	1.8	N/A
O	3.5	4.3	3.6	5.6	N/A
H_{NH_3}	1.0	1.1	1.0	1.0	1.2
H_{NH}	1.0	1.0	1.0	1.0	0.9
O_{CO}	2.4	2.4	2.0	1.9	1.0
O_{CO_2}	3.3	3.7	3.4	3.1	3.6

numbers for hydrogen bonding in the first solvation shell⁶⁴ are given in Table 5. The naming scheme for atom types is shown in Figure 1a. Overall, the charge set MDRF performs clearly better than the set MDR. For the $\text{O}-\text{H}_\text{W}$ radial distribution function (Figure 3b), both charge sets yield a first peak that is shifted to a shorter distance by ≈ 0.06 Å compared to the QM/MM reference. Thus, both charge sets somewhat overestimate the basicity of the O atoms. However, MDRF charges yield a first peak that is merely shifted, with the shape of the peak and the hydrogen-bond coordination number N_C (Table 5) being in good agreement with QM/MM. In contrast, MDR charges lead to a broadening of the peak and severe overestimation of N_C . The shape and depth of the first minimum around 2.4 Å indicates that the orientation of water molecules in the first solvation shell is

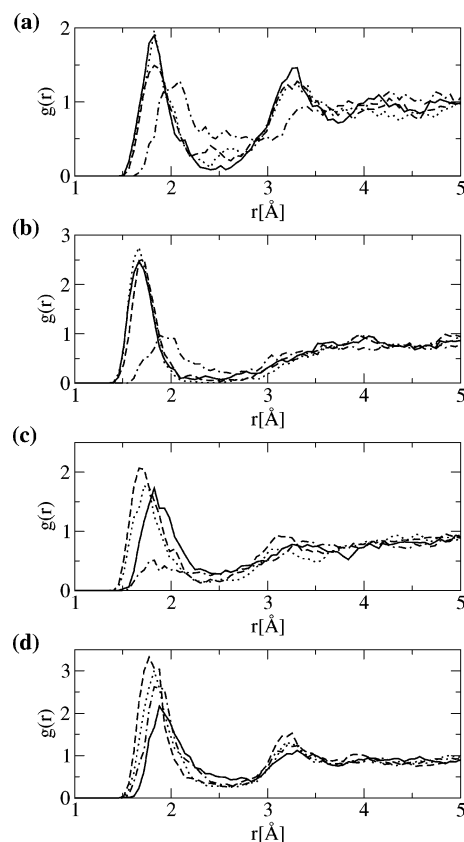


Figure 4. Radial distribution functions $g(r)$ of polar groups of the Gly-Ala dipeptide. The line convention is the same as in Figure 3. Dashed-dotted lines refer to a simulation using original GROMOS parameters. Shown are the radial distribution functions (a) $\text{H}_{\text{NH}_3}-\text{O}_\text{W}$, (b) $\text{H}_{\text{NH}}-\text{O}_\text{W}$, (c) $\text{O}_{\text{CO}}-\text{H}_\text{W}$, and (d) $\text{O}_{\text{CO}_2}-\text{H}_\text{W}$.

more rigid in the QM/MM and MDRF simulations compared to that in the simulation with MDR charges.

Significant differences are also found in the solvation of the hydroxyl group. The $\text{H}-\text{O}_\text{W}$ radial distribution function in Figure 3a shows excellent agreement between MDRF and the QM/MM reference, while MDR charges severely underestimate the acidity of the protons. In the case of the hydroxyl oxygen atoms O_H , MDR charges qualitatively fail to reproduce the small first peak (Figure 3c). In contrast, MDRF charges slightly overestimate hydrogen bonding to the solvent, but the solvation structure is in overall good agreement with the QM/MM reference. Since there is no well-defined first solvation shell in the case of the O_H atoms, a comparison of coordination numbers does not appear to be meaningful.

Solute-solvent radial distribution functions $g(r)$ of polar groups of the Gly-Ala dipeptide are shown in Figure 4; the corresponding coordination numbers for hydrogen bonding⁶⁴ are given in Table 5. As in the case of H_2PO_4^- , the solvation of hydrogen-bond donors is reproduced better than that of acceptors. MDRF charges in fact reproduce the solvation of the terminal NH_3^+ group almost perfectly. MDR charges on the other hand underestimate the height of the first peak of the $\text{H}_{\text{NH}_3}-\text{O}_\text{W}$ radial distribution function but correctly reproduce the position of the first maximum. Both charge sets reproduce well the position and width of the second peak

at 3.3 Å. For the solvation of the hydrogen H_{NH} in the amide bond, the agreement with the QM/MM reference is excellent for both of the fitted charge sets.

The hydrogen-bond acceptor strengths of the carbonyl and carboxyl oxygens are clearly overestimated by both charge sets, with MDRF performing slightly better than MDR. In the case of the terminal carboxylate group, the best agreement with the QM/MM reference of all classical simulations is obtained with the original GROMOS parameters. For the other polar groups, however, we observe a clear improvement compared to GROMOS charges by using the fitted charge sets.

Since Lennard-Jones interactions are identical in the QM/MM and classical simulations, the shifts in $g(r)$ involving oxygen atoms must be attributed to an inability of the classical model to reproduce the charge distribution found in QM/MM. Most likely, the major flaw of the classical model consists in the use of atom-centered point charges that do not allow to account for anisotropies of the charge distribution around an atom. In addition, it appears that polarization of the QM/MM charge density also leads to an overestimation of hydrogen-bond acceptor capabilities. This view is supported by the following observation: gas-phase derived RESP charges still lead to an overestimation of the acceptor capability of the Gly-Ala oxygen atoms, but to a lesser extent than MDR(F) charges (Figure S-2, Supporting Information). In fact, we expect the charge distribution to be less anisotropic in the gas phase compared to that in the hydrated species, where the lone pairs will be strongly oriented toward the protons of the first hydration shell. On the other hand, RESP charges significantly underestimate the acidity of the proton of the amide group of Gly-Ala (Figure S-2, Supporting Information). In the case of $H_2PO_4^-$, charges derived in the gas phase underestimate the acidity of the protons and overestimate the basicity of the oxygen atoms. This result can be attributed to a charge distribution that is rather diffuse in the gas phase, while explicit hydration leads to a stronger localization of the charge. Consequently, charges derived from a polarized charge density give a better description of the solvation structure.

In view of the above observations, it appears crucial for an accurate description of the solvation structure of polar groups that the charges be derived from a QM/MM wavefunction that is polarized by the solvent. For some acceptor groups, however, polarization leads to an overestimation of hydrogen bonding, as in the case of the oxygen atoms of Gly-Ala. The inclusion of off-atomic interaction sites, such as lone pairs, should lead to a better description of hydrogen-bond acceptors.^{28,60}

In the case of TNDM, the only hydrophilic groups are the carboxyl ligands, the solvation structure of which is reproduced well (Supporting Information, Figure S-1). In contrast to $H_2PO_4^-$ and Gly-Ala, hydrogen bonding of the oxygen atoms is slightly underestimated. The remaining groups are of hydrophobic character, which is well-reproduced by the optimized parameters in the case of the aliphatic groups. The optimized charge sets also reproduce the hydrophobic character of the nitrosyl and carbonyl ligands. In fact, they appear slightly more hydrophobic in

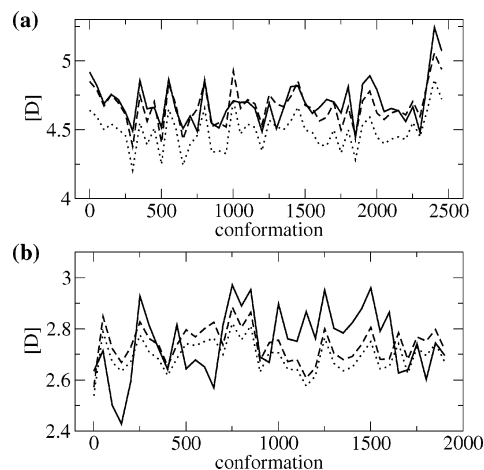


Figure 5. Dipole moments (in Debye) for conformations along the QM/MM reference trajectory. Shown are the dipole moment in the QM/MM simulation (solid lines) and dipole moments calculated with MDR (dashed lines) and MDRF charge sets (dotted lines). The corresponding average values and standard deviations are given in Table 6. (a) Gly-Ala dipeptide. (b) TNDM.

Table 6. Average and Standard Deviation of the Dipole Moment along the QM/MM Reference Trajectory (in Debye)

	Gly-Ala	TNDM
QM/MM	4.69 ± 0.15	2.72 ± 0.15
MDR	4.66 ± 0.13	2.71 ± 0.08
MDRF	4.48 ± 0.12	2.67 ± 0.08

the classical simulations than in the QM/MM reference, where we find a more pronounced peak at around 3 Å in the O–O_w radial distribution function (Figure S-1, Supporting Information).

3.2.2. Dipole Moments. An additional test to assess the quality of the fitted charge sets consists in comparing the total dipole moment of the solute to that of the QM/MM reference. Figure 5 compares the quantum mechanical dipole moments in conformations taken from the QM/MM reference simulation to the equivalent quantity as described with MDR and MDRF charge sets. Averages and standard deviations are reported in Table 6.

In general, the dipole moment is reproduced well by both charge sets, with absolute deviations below 0.4 D (0.3 D for TNDM), corresponding to relative deviations below 10%. The average dipole of MDR charges agrees within 0.03 D (i.e., better than 1%) with the QM/MM reference. MDRF charges, on the other hand, systematically underestimate the dipole, especially in the case of Gly-Ala. The smaller fluctuations in the classical simulations compared to the QM/MM reference must be attributed to the fixed charge model, as changes of the dipole moment arise from changes of the molecular geometry only. In the QM/MM simulations, on the other hand, there is an additional contribution from instantaneous charge fluctuations.

It becomes apparent from Figure 5 that MDR charges perform clearly better than MDRF charges, not only in reproducing the average dipole but also in reproducing the

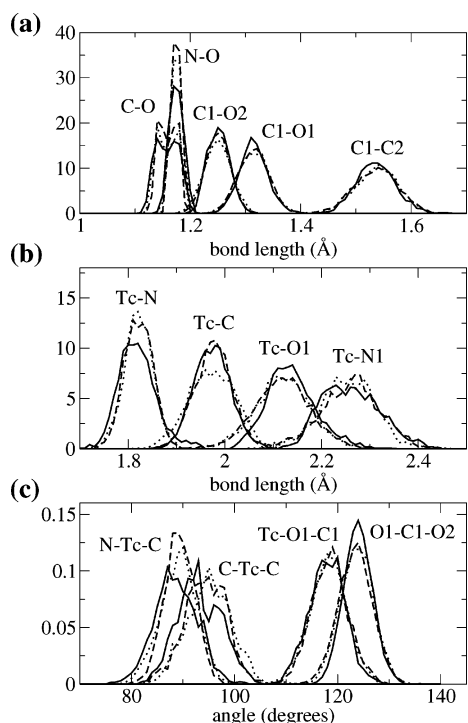


Figure 6. Normalized distribution of (a, b) selected bond lengths and (c) selected bond angles in TNM. The line convention is identical to that in Figure 3. The atom naming convention for atom types is shown in Figure 1c.

dipole fluctuations along the trajectory. This can be interpreted as an effect of the different charge-fitting procedures. Including the electric field in the fitting leads to a better description at short range, because of the $1/r^2$ dependence of the field. Evidently, this is achieved at the expense of a poorer quality at longer range, compared to fitting of the potential only (Figure 2). Including the field in the fitting procedure apparently leads to a different weighting of the fitting, in the sense that the optimized charges represent well the electronic properties of functional groups but to a lesser extent those of the entire molecule. Thus, MDRF charges perform better in reproducing more “local” properties, such as the structure of the first solvation shell around a functional group, while MDR charges perform better for more “global” properties like the total dipole moment. A possible way to overcome these limitations of MDRF charges could consist in explicitly including the dipole moment (and possibly higher multipoles) in the fitting procedure.

3.2.3. Molecular Structures. We will limit the discussion of structural properties to TNM, as it presents the most challenging features for a force-matching approach to reproduce. However, the results obtained for TNM are representative also for the other two test compounds. The naming convention for the atom types of TNM is shown in Figure 1c. Figure 6 shows normalized distributions of selected bond lengths and bond angles in the QM/MM reference simulation and in the simulations with optimized parameters. The overall agreement can be considered excellent, both for the position of the maximum and the width of the distribution. The small differences in length and strength of the bond in the CO and NO⁺ ligands are reproduced faithfully by both parameter sets. The same observation holds

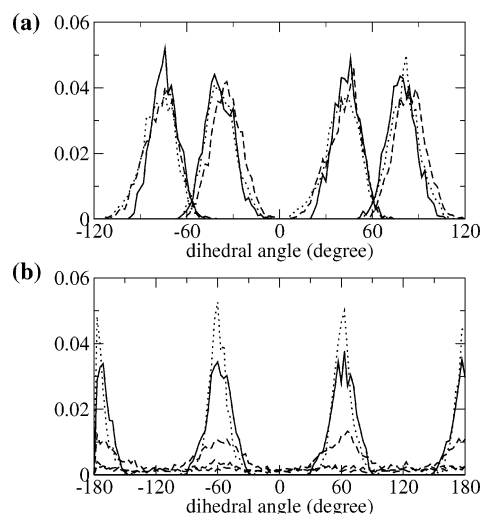


Figure 7. Normalized distribution of selected dihedral angles in TNM. (a) C3–N1–C2–H_{C2}. (b) Tc–N1–C3–H_{C3}. The line convention is identical to that in Figure 3.

for the different metal–ligand bonds. The method also captures the different C–O bond lengths in the carboxyl ligand. Both parameter sets yield almost identical distributions, with the exception of the metal–carbonyl bond, the strength of which is underestimated by the MDRF parameter set. For the MDR parameters, on the other hand, we find a distribution for this bond that is practically identical to the QM/MM reference. The difference most likely results from the different intramolecular electrostatic interaction between the carbonyl and carboxyl ligands, for which the two charge-fitting schemes yield rather different charges (Table 3).

Figure 7a shows normalized distributions of the four dihedral angles C3–N1–C2–H_{C2}. These dihedrals are part of a rigid ring system resulting from chelation of the metal center by the ligand. All four distributions are well-reproduced by both fitted parameter sets. The picture looks different for the N1–C3 bond, which is the only bond in TNM around which rotation can occur. Figure 7b shows distributions of the three dihedral angles Tc–N1–C3–H_{C3}, for which the minima of the torsional potential are reproduced correctly. However, while there are no dihedral transitions in the QM/MM reference simulation, they do occur in the simulation with the parameter set MDR, clearly indicating that the height of the rotational barrier is underestimated in the fitting process. In contrast, no dihedral transitions occur with MDRF parameters and the distribution is reproduced remarkably well. This indicates a value for the torsional barrier that is closer to the “true” value in the QM/MM description. In fact, the narrower distribution indicates that the barrier height is slightly overestimated with MDRF. For a quantitative assessment, one would need to compare the frequency at which dihedral transitions occur, which in turn requires simulation times of sufficient length to observe a significant number of these events. Unless enhanced sampling techniques are used, the necessary simulation time is beyond what can currently be achieved with reasonable computational effort within a DFT/MM approach.

4. Conclusions

We introduce a force-matching approach to derive parameters for nonpolarizable biomolecular force fields from QM/MM simulations. As a consequence of using QM/MM calculations for obtaining the reference forces, the parameters are derived for a species that is explicitly polarized by the environment, and finite temperature and pressure are automatically taken into account. We have optimized all interaction parameters except those for van der Waals interactions, which are retained from the classical force field. This choice is made in order to remain consistent with the QM/MM Hamiltonian¹³ but is also dictated by the failure of DFT to account for dispersion interactions.

MD simulations with optimized parameters perform remarkably well in reproducing properties from the QM/MM simulation. The agreement can certainly be improved further by using a more sophisticated force field, for example, by including lone pairs as additional interaction sites or by abandoning the fixed point-charge description for an explicitly polarizable model. In fact, our procedure can point out the necessity for using a more sophisticated model and allows quantification of the improvement brought about by such a model. For example, the results presented here suggest that a fluctuating charge model with atomic point charges as the sole interaction sites is insufficient for significantly improving the description of electrostatics, at least for the systems considered here and if the ability to reproduce the electrostatic field is taken as a measure.

The charge scheme MDRF is slightly, sometimes clearly, superior to its counterpart MDR in reproducing solvation structures. For O_H in H_2PO_4^- , MDR fails to describe the correct (QM/MM) solvation structure, while MDRF gives excellent agreement. For larger molecules, a charge-fitting procedure aimed at reproducing the forces on the MM atoms that are close to the QM subsystem might become inappropriate, as charges of QM atoms that are far from the QM/MM boundary will become ill-defined. In these cases, it might be necessary to combine the derivation of bonded and nonbonded parameters into a single, necessarily nonlinear, minimization scheme. As a benefit, such an approach could also lead to an improved balance between electrostatic and covalent intramolecular interaction parameters.

An obvious drawback of using DFT for the reference calculations lies in its failure to describe dispersion interactions within the quantum system, so that the parametrization of Lennard-Jones potentials is not possible within a standard QM/MM scheme based on a purely local approximation to DFT. The recent development of dispersion-corrected pseudopotentials⁶⁵ might open a way to overcome this limitation and develop a “DFT-consistent” force field including Lennard-Jones parameters. A further limitation concerns the derivation of torsional barriers, since the time scale that is accessible to the QM/MM reference simulation will in general be insufficient for the sampling of complete torsional profiles. This limitation could be overcome by exploiting an enhanced sampling technique.^{33–36}

Since the parameters are derived for a specific environment, the method could be very useful in the context of free energy perturbation methods for the accurate determination

of receptor/ligand binding free energies. For these applications, the ligand (and the receptor binding site) could be parametrized in several states along the reaction coordinate, providing an accurate estimate of the binding free energy that can account for long-time fluctuations of the protein environment. The method appears to be ideally suited to parametrize compounds whose stability is crucially influenced by the environment, such as reaction intermediates in enzymatic cycles. The method can further serve as a tool to analyze the influence of the environment on charge distributions or bond strengths.

Currently, the method is being applied to study the binding of ruthenium and platinum anticancer drugs to DNA.^{66,67} Results of these studies will be published in separate articles.^{68,69}

Acknowledgment. We thank the Swiss Center for Scientific Computing (CSCS) in Manno, Switzerland, for a generous allocation of CPU time. This work was supported by the Swiss National Science Foundation (Grant No. 21.57250.99).

Supporting Information Available: The solvation structure of H_2PO_4^- and Gly-Ala using HF/6-31+G*-derived charges (Figures S-1 and S-2), the solvation structure of TNDM (Figure S-3), and CPU requirements for QM/MM and classical simulations (Table S-1). This material is available free of charge via the Internet at <http://pubs.acs.org>.

References

- (1) Hansson, T.; Oostenbrink, C.; van Gunsteren, W. F. *Curr. Opin. Struct. Biol.* **2002**, *12*, 190–196.
- (2) van Gunsteren, W. F.; Billeter, S. R.; Eising, A. A.; Hünenberger, P. H.; Krüger, P.; Mark, A. E.; Scott, W. R. P.; Tironi, I. G. *Biomolecular Simulation: The GROMOS96 Manual and User Guide*; vdf Hochschulverlag AG: Zürich, 1996.
- (3) Cornell, W. D.; Cieplak, P.; Bayly, C. I.; Gould, I. R.; Merz, K. M., Jr.; Ferguson, D. M.; Spellmeyer, D. C.; Fox, T.; Caldwell, J. W.; Kollman, P. A. *J. Am. Chem. Soc.* **1995**, *117*, 5179–5197.
- (4) Jorgensen, W. L.; Maxwell, D. S.; Tirado-Rives, J. *J. Am. Chem. Soc.* **1996**, *118*, 11225–11236.
- (5) MacKerell, A. D., Jr.; Bashford, D.; Bellott, R. L.; Dunbrack, R. L., Jr.; Evanseck, J. D.; Field, M. J.; Fischer, S.; Gao, J.; Guo, H.; Ha, S.; Joseph-McCarthy, D.; Kuchnir, L.; Kuczera, K.; Lau, F. T. K.; Mattos, C.; Michnick, S.; Ngo, T.; Nguyen, D. T.; Prodhom, B.; Reiher, W. E., III; Roux, B.; Schlenkrich, M.; Smith, J. C.; Stote, R.; Straub, J.; Watanabe, M.; Wiorkiewicz-Kuczera, J.; Yin, D.; Karplus, M. *J. Phys. Chem. B.* **1998**, *102*, 3586–3616.
- (6) Ponder, J. W.; Case, D. A. *Adv. Protein Chem.* **2003**, *66*, 27–85.
- (7) MacKerell, A. D., Jr. *J. Comput. Chem.* **2004**, *25*, 1584–1604.
- (8) Bayly, C. I.; Cieplak, P.; Cornell, W. D.; Kollman, P. A. *J. Phys. Chem.* **1993**, *97*, 10269–10280.
- (9) Warshel, A.; Levitt, M. *J. Mol. Biol.* **1976**, *103*, 227–249.
- (10) Singh, U. C.; Kollman, P. A. *J. Comput. Chem.* **1986**, *7*, 718–730.

- (11) Field, M. J.; Bash, P. A.; Karplus, M. *J. Comput. Chem.* **1990**, *11*, 700–733.
- (12) Eichinger, M.; Tavan, P.; Hutter, J.; Parrinello, M. *J. Chem. Phys.* **1999**, *110*, 10452–10467.
- (13) Laio, A.; VandeVondele, J.; Rothlisberger, U. *J. Chem. Phys.* **2002**, *116*, 6941–6947.
- (14) Laio, A.; Bernard, S.; Chiarotti, G. L.; Scandolo, S.; Tosatti, E. *Science* **2000**, *287*, 1027–1030.
- (15) Csányi, G.; Albaret, T.; Payne, M. C.; De Vita, A. *Phys. Rev. Lett.* **2004**, *93*, 175503.
- (16) Ercolessi, F.; Adams, J. B. *Europhys. Lett.* **1994**, *26*, 583–588.
- (17) Lenosky, T. J.; Sadigh, B.; Alonso, E.; Bulatov, V. V.; Diaz de la Rubia, T.; Kim, J.; Voter, A. F.; Kress, J. D. *Modell. Simul. Mater. Sci. Eng.* **2000**, *8*, 825–841.
- (18) Umeno, Y.; Kitamura, T.; Date, K.; Hayashi, M.; Iwasaki, T. *Comput. Mater. Sci.* **2002**, *25*, 447–456.
- (19) Li, Y.; Siegel, D. J.; Adams, J. B.; Liu, X.-Y. *Phys. Rev. B: Condens. Matter Mater. Phys.* **2003**, *67*, 125101.
- (20) Aguado, A.; Madden, P. A. *J. Chem. Phys.* **2003**, *118*, 5718–5728.
- (21) Aguado, A.; Madden, P. A. *Phys. Rev. B: Condens. Matter Mater. Phys.* **2004**, *70*, 245103.
- (22) Izvekov, S.; Parrinello, M.; Burnham, C. J.; Voth, G. A. *J. Chem. Phys.* **2004**, *120*, 10896–10913.
- (23) Rick, S. W.; Berne, B. J. *J. Am. Chem. Soc.* **1996**, *118*, 672–679.
- (24) Liu, Y.-P.; Kim, K.; Berne, B. J.; Friesner, R. A.; Rick, S. W. *J. Chem. Phys.* **1998**, *108*, 4739–4755.
- (25) Banks, J. L.; Kaminski, G. A.; Zhou, R.; Mainz, D. T.; Berne, B. J.; Friesner, R. A. *J. Chem. Phys.* **1999**, *110*, 741–754.
- (26) Wang, J.; Cieplak, P.; Kollman, P. A. *J. Comput. Chem.* **2000**, *21*, 1049–1074.
- (27) Ferenczy, G. G.; Reynolds, C. A. *J. Phys. Chem. A* **2001**, *105*, 11470–11479.
- (28) Cieplak, P.; Caldwell, J.; Kollman, P. A. *J. Comput. Chem.* **2001**, *22*, 1048–1057.
- (29) Tabacchi, G.; Mundy, C. J.; Hutter, J.; Parrinello, M. *J. Chem. Phys.* **2002**, *117*, 1416–1433.
- (30) Kaminski, G. A.; Stern, H. A.; Berne, B. J.; Friesner, R. A.; Cao, Y. X.; Murphy, R. B.; Zhou, R.; Halgren, T. A. *J. Comput. Chem.* **2002**, *23*, 1515–1531.
- (31) Kaminski, G. A.; Stern, H. A.; Berne, B. J.; Friesner, R. A. *J. Phys. Chem. A* **2004**, *108*, 621–627.
- (32) Patel, S.; MacKerell, A. D., Jr.; Brooks, C. L., III. *J. Comput. Chem.* **2004**, *25*, 1504–1514.
- (33) Carter, E. A.; Ciccotti, G.; Hynes, J. T.; Kapral, R. *Chem. Phys. Lett.* **1989**, *156*, 472–477.
- (34) VandeVondele, J.; Rothlisberger, U. *J. Chem. Phys.* **2000**, *113*, 4863–4868.
- (35) VandeVondele, J.; Rothlisberger, U. *J. Phys. Chem. B* **2002**, *106*, 203–208.
- (36) Laio, A.; Parrinello, M. *Proc. Natl. Acad. Sci. U.S.A.* **2002**, *99*, 12562–12566.
- (37) Laio, A.; VandeVondele, J.; Rothlisberger, U. *J. Phys. Chem. B* **2002**, *106*, 3700–3707.
- (38) Hirshfeld, F. L. *Theor. Chim. Acta* **1977**, *44*, 129–138.
- (39) Reynolds, C. A.; Essex, J. W.; Richards, W. G. *J. Am. Chem. Soc.* **1992**, *114*, 9075–9079.
- (40) With a cutoff of 8 Å, the number of NN atoms in a single conformation is typically on the order of a few hundred.
- (41) Lawson, C. L.; Hanson, R. J. *Solving Least Squares Problems*; Prentice Hall: Englewood Cliffs, NJ, 1974.
- (42) Moré, J. J. The Levenberg–Marquardt Algorithm: Implementation and Theory. In *Numerical Analysis*; Watson, G. A., Ed.; Springer-Verlag: New York, 1977; pp 105–116.
- (43) Moré, J. J.; Garbow, B. S.; Hillstom, K. E. *User Guide for MINPACK-1*; Report ANL-80-74; Argonne National Laboratory: Argonne, IL, 1980.
- (44) Hugosson, H. W.; Laio, A.; Maurer, P.; Rothlisberger, U. *J. Comput. Chem.* **2006**, *27*, 672–684.
- (45) Dilworth, J. R.; Parrott, S. J. *Chem. Soc. Rev.* **1998**, *27*, 43–55.
- (46) Schibli, R.; Schubiger, P. A. *Eur. J. Nucl. Med.* **2002**, *29*, 1529–1542.
- (47) Car, R.; Parrinello, M. *Phys. Rev. Lett.* **1985**, *55*, 2471–2474.
- (48) CPMD, v. 3.8; IBM Corp: Armonk, NY, 1990–2004. Copyright MPI fuer Festkoerperforschung Stuttgart 1997–2001.
- (49) Scott, W. P. R.; Hünenberger, P. H.; Tironi, I. G.; Mark, A. E.; Billeter, S. R.; Fennen, J.; Torda, A. E.; Huber, T.; Krüger, P.; van Gunsteren, W. F. *J. Phys. Chem. A* **1999**, *103*, 3596–3607.
- (50) Trouiller, N.; Martins, J. L. *Phys. Rev. B: Condens. Matter Mater. Phys.* **1991**, *43*, 1993–2006.
- (51) Becke, A. D. *Phys. Rev. A: At., Mol., Opt. Phys.* **1988**, *38*, 3098–3100.
- (52) Lee, C.; Yang, W.; Parr, R. G. *Phys. Rev. B: Condens. Matter Mater. Phys.* **1988**, *37*, 785–789.
- (53) Berendsen, H. J. C.; Postma, J. P. M.; van Gunsteren, W. F.; Hermans, J. Interaction Models for Water in Relation to Protein Hydration. In *Intermolecular Forces*; Pullman, B., Ed.; Reidel: Dordrecht, The Netherlands, 1981; pp 331–342.
- (54) Perdew, J. P. *Phys. Rev. B: Condens. Matter Mater. Phys.* **1986**, *33*, 8822–8824.
- (55) Maurer, P.; Magistrato, A.; Rothlisberger, U. *J. Phys. Chem. A* **2004**, *108*, 11494–11499.
- (56) Jorgensen, W. L.; Chandrasekhar, J.; Madura, J. D.; Impey, R. W.; Klein, M. L. *J. Chem. Phys.* **1983**, *79*, 926–935.
- (57) Frisch, M. J.; Trucks, G. W.; Schlegel, H. B.; Scuseria, G. E.; Robb, M. A.; Cheeseman, J. R.; Montgomery, J. A., Jr.; Vreven, T.; Kudin, K. N.; Burant, J. C.; Millam, J. M.; Iyengar, S. S.; Tomasi, J.; Barone, V.; Mennucci, B.; Cossi, M.; Scalmani, G.; Rega, N.; Petersson, G. A.; Nakatsuji, H.; Hada, M.; Ehara, M.; Toyota, K.; Fukuda, R.; Hasegawa, J.; Ishida, M.; Nakajima, T.; Honda, Y.; Kitao, O.; Nakai, H.; Klene, M.; Li, X.; Knox, J. E.; Hratchian, H. P.; Cross, J. B.; Bakken, V.; Adamo, C.; Jaramillo, J.; Gomperts, R.; Stratmann, R. E.; Yazyev, O.; Austin, A. J.; Cammi, R.; Pomelli, C.; Ochterski, J. W.; Ayala, P. Y.; Morokuma, K.; Voth, G. A.; Salvador, P.; Dannenberg, J. J.; Zakrzewski, V. G.; Dapprich, S.; Daniels, A. D.; Strain, M. C.; Farkas, O.; Malick, D. K.; Rabuck, A. D.; Raghavachari, K.

- Foresman, J. B.; Ortiz, J. V.; Cui, Q.; Baboul, A. G.; Clifford, S.; Cioslowski, J.; Stefanov, B. B.; Liu, G.; Liashenko, A.; Piskorz, P.; Komaromi, I.; Martin, R. L.; Fox, D. J.; Keith, T.; Al-Laham, M. A.; Peng, C. Y.; Nanayakkara, A.; Challacombe, M.; Gill, P. M. W.; Johnson, B.; Chen, W.; Wong, M. W.; Gonzalez, C.; Pople, J. A. *Gaussian 03*, revision B.03; Gaussian Inc.: Pittsburgh, PA, 2003.
- (58) Case, D. A.; Darden, T. A.; Cheatham, T. E., III; Simmerling, C. L.; Wang, J.; Duke, R. E.; Luo, R.; Merz, K. M.; Wang, B.; Pearlman, D. A.; Crowley, M.; Brozell, S.; Tsui, V.; Gohlke, H.; Mongan, J.; Hornak, V.; Cui, G.; Beroza, P.; Schafmeister, C.; Caldwell, J. W.; Ross, W. S.; Kollman, P. A. *AMBER 8*; University of California: San Francisco, CA, 2004.
- (59) Rappé, A. K.; Goddard, W. A., III. *J. Phys. Chem.* **1991**, *95*, 3358–3363.
- (60) Masia, M.; Probst, M.; Rey, R. *J. Chem. Phys.* **2004**, *121*, 7362–7378.
- (61) The very large deviation of the potential below 1.7 Å results from a small fraction of atoms (less than 10 out of several thousand). The small number makes them essentially irrelevant for the fitting.
- (62) D-RESP charges correspond to MDR charges but are derived for a single conformation and with a stronger restraint to the Hirshfeld values ($w^H = 0.1$). The stronger restraint represents a compromise between avoiding large charge fluctuations between conformations and achieving a good quality of the fit. See ref 37 for details.
- (63) Starting from an existing parametrization of H_3PO_4 (Spieser, S. A. H.; Leeftang, B. R.; Kroon-Batenburg, L. M. J.; Kroon, J. J. *J. Chem. Phys. A* **2000**, *104*, 7333–7338), charges were adjusted manually in order to reproduce the solvation structure of a QM/MM reference. Colombo, M. C.; Vande-Vondele, J.; Rothlisberger, U. To be published.
- (64) The first solvation shell is assumed to extend up to 2.5 Å.
- (65) von Lilienfeld, O. A.; Tavernelli, I.; Rothlisberger, U.; Sebastiani, D. *Phys. Rev. Lett.* **2004**, *93*, 153004.
- (66) Dorcier, A.; Dyson, P. J.; Gossens, C.; Rothlisberger, U.; Scopelliti, R.; Tavernelli, I. *Organometallics* **2005**, *24*, 2114–2123.
- (67) Spiegel, K.; Rothlisberger, U.; Carloni, P. *J. Phys. Chem. B* **2004**, *108*, 7963–7968.
- (68) Gossens, C.; Tavernelli, I.; Maurer, P.; Rothlisberger, U. To be published.
- (69) Spiegel, K.; Magistrato, A.; Maurer, P.; Ruggerone, P.; Rothlisberger, U.; Carloni, P.; Reedijk, J.; Klein, M. Submitted for publication.

CT600284F